Physics of Plasmas

ITER cold VDEs in the limit of perfectly conducting walls

Cite as: Phys. Plasmas **28**, 012511 (2021); https://doi.org/10.1063/5.0037464
Submitted: 13 November 2020 • Accepted: 03 January 2021 • Published Online: 21 January 2021

C. F. Clauser and S. C. Jardin

ITER cold VDEs in the limit of perfectly conducting walls

Cite as: Phys. Plasmas **28**, 012511 (2021); doi: 10.1063/5.0037464
Submitted: 13 November 2020 · Accepted: 3 January 2021 ·
Published Online: 21 January 2021

C. F. Clauser[a)] and S. C. Jardin

AFFILIATIONS

Princeton Plasma Physics Laboratory, Princeton, New Jersey 08543, USA

[a)]Author to whom correspondence should be addressed: cclauser@pppl.gov

ABSTRACT

Recently, it has been shown that a vertical displacement event (VDE) can occur in ITER even when the walls are perfect conductors, as a consequence of the current quench (CQ) [A. H. Boozer, Phys. Plasmas **26,** 114501 (2019)]. We used the extended-MHD code M3D-C^1 with an ITER-like equilibrium and induced a CQ to explore cold VDEs in the limit of perfectly conducting walls, using different wall geometries. In the case of a rectangular first wall with the side walls far away from the plasma, we obtained very good agreement with the analytical model developed by Boozer that considers a top/bottom flat-plates wall. We show that the solution in which the plasma remains at the initial equilibrium position is improved when bringing the side walls closer to the plasma. When approximating the ITER first wall as a perfect conductor, the plasma remains stable at the initial equilibrium position far beyond the value predicted by the flat-plates wall limit. When considering an opposite limit in which only the inner shell of the ITER vacuum vessel acts as a perfect conductor, the plasma is displaced during the CQ, but the edge safety factor remains above 2 longer in the current decay compared to the flat-plates wall limit. In all the simulated cases, the VDE is found to be strongly dependent on the plasma current, in agreement with a similar finding in the flat-plates wall limit, showing an important difference with hot VDEs in which the CQ is not a necessary condition.

I. INTRODUCTION

Vertical Displacement Events (VDEs) are major disruptions that occur in elongated tokamak plasmas (see, for example, Ref. 1). Reliable simulations to predict possible scenarios in ITER are essential. In a "cold VDE," the disruption thermal quench (TQ) occurs when the plasma is still at the equilibrium position, and then the plasma displaces upward or downward.[2] This is in contrast to a "hot VDE" in which the hot plasma column displaces vertically due to the loss of position control, and the thermal quench occurs later as a result of the plasma contacting the first wall. Both of these events are expected to occur in ITER and they each develop heat and force loads that will stress the structure in different ways.

The actual ITER conducting structure is complicated as discussed in Ref. 3. The first wall will have poor toroidal conductivity since it is made of panels with gaps between them. The solid inner shell of the vacuum vessel is removed from the first wall by about 60 cm and has very good toroidal conductivity. In between the first wall and the vacuum vessel are complex 3D blanket modules that are conducting but do not provide a continuous toroidal path. However, it has been pointed out[4] that if the plasma fills the gaps in the first wall during a disruption event, it might short circuit the first wall making it toroidally conducting. More recently, Boozer[5] has considered the limiting case in which the ITER first wall acts as a perfect conductor and, approximating it as two top/bottom flat plates, has shown that, even in this perfectly conducting wall limit, a current quench (CQ) could drive a VDE. In this situation, active controls would not be applicable since the magnetic fields cannot penetrate the wall in the required timescale. In addition, this simple model, which will be referred to here as the flat-plates wall limit, shows that the edge safety factor could drop down to values around $q_{95} \sim 2$ even when the plasma current is still large. This condition could lead to large and unacceptable halo currents and local force densities in the first wall.[5]

In this study, we use the M3D-C^1 code to simulate cold VDEs in the limit of perfectly conducting walls. We represent the conducting structure as axisymmetric and consider two limiting cases: (1) the first wall is a perfect conductor or (2) the first wall and blanket modules are insulators and the vacuum vessel is a perfect conductor. For case (1), we also consider different geometries and show that in this limit, the ITER first wall keeps the plasma centered far beyond the value predicted by the flat-plates wall limit. However, for case (2), when assuming that the perfectly conducting structure is the inner shell of the ITER vacuum vessel, the plasma is displaced during the current quench but the safety factor should not decrease as fast as in the flat-plates wall limit.

This paper is organized as follows: in Sec. II, we present the plasma equilibrium and the different wall geometries employed. In Sec. III, we show the limiting case in which the flat-plates wall limit is applicable. Finally, we show in Sec. V the results using the ITER first wall as a perfect conductor as well as the case in which only the inner shell of ITER vacuum vessel acts as a perfect conductor.

II. NUMERICAL MODEL

We started the simulations from a standard ITER-like equilibrium with plasma current $I = 15\,\text{MA}$, vacuum magnetic field $B_0 = 5.3\,\text{T}$, internal inductance $l_i(3) = 0.816$, magnetic axis $(R_m, Z_m) = (6.524\,\text{m}, 0.537\,\text{m})$, an active lower x-point at $(R,Z) = (5.148\,\text{m}, -3.386\,\text{m})$, and a passive upper x-point at $(R,Z) = (6.618\,\text{m}, 4.748\,\text{m})$. The equilibrium is the same as the one used in Ref. 6, which provides more detailed information, and Ref. 7. The plasma central temperature is $\sim$30 keV (the temperature is the same for electrons and ions) and boundary temperature is set to a constant value of 0.169 eV. All the cases presented in this study start from the same equilibrium.

M3D-C^1 (Refs. 8 and 9) is a high order finite-element code that solves the extended-MHD equations in a plasma region (P). It has also been extended to include a (resistive) wall region (W) and a vacuum region (V),[10] and external coils are included to calculate the initial equilibrium. These regions and the meshes are shown in Fig. 1. The code was successfully employed to study VDEs in tokamaks in both 2D and 3D.[7,11] In support of this capability, a benchmark in 2D with well-known codes NIMROD[12] and JOREK[13] was recently carried out with success.[14] In this study, we use the 2D version of M3D-C^1 and we employed different wall geometries: (a) a thin rectangular wall, (b) a thin ITER first wall, and (c) a thick two-layer ITER wall. We note here that M3D-C^1 can handle only closed contours around the plasma as a resistive wall. Note also that the "thin" walls were of thickness 2–6 cm with finite elements in the wall.

For the rectangular geometry, Fig. 1(a), we scanned over three different cases R1, R2, and R3: the former with the side walls far away from the plasma but inside the coil region and the latter with the side walls very close to the plasma. The wall resistivity employed in the rectangular geometries as well as in the thin ITER wall geometry, Fig. 1(b), was $\eta_w = 3.6 \times 10^{-8}\,\Omega\,\text{m}$, which is similar to the resistivity of Beryllium and approximates an ideal conducting wall on the time-scales of these calculations.

The last case, Fig. 1(c), shows a new capability that has been recently incorporated in M3D-C[1]: a resistive wall region with different layers in which anisotropic wall resistivities can also be set. This new model is an important step toward more realistic simulations of resistive wall instabilities. The plasma–wall interface matches the ITER first wall as in the $I1$ model, and the W1 region represents the ITER first wall panels and blanket modules. As mentioned before, in ITER, the first wall panels are expected to have a poor toroidal conductivity. The W2 region constitutes the ITER inner vacuum vessel shell, which is a very good conductor. As a limiting case for the present study and, in contrast to the models R1–3 and I1, we also explored the situation in which the W1 region acts as an insulator while the W2 region acts as a perfect conductor. We set the W1 region to have a resistivity of $\eta_{w1} = 1.933 \times 10^{-2}\,\Omega\,\text{m}$, while in the W2 region, $\eta_{w2} = 3.6 \times 10^{-8}\,\Omega\,\text{m}$. With this election, the W1 region will not play a significant role, but it will limit the plasma movement. On the other hand, all the toroidal wall induction due to the plasma dynamics will develop in the W2 region.

All these simulations were performed in 2D using the single temperature MHD model described in Ref. 15. To facilitate the discussion in Secs. III and IV, we introduce here the primary terms in the temperature equation that is solved in the plasma region:

$$\frac{3}{2} n \frac{\partial T}{\partial t} = -\nabla \cdot \mathbf{q} + \eta \mathbf{J}^2 + (\cdots), \tag{1a}$$

$$\mathbf{q} = -\kappa_\perp \nabla_\perp T - \kappa_\parallel \nabla_\parallel T. \tag{1b}$$

Here, $\eta \sim T^{-3/2}$ is the Spitzer resistivity, which can be scaled by an arbitrary constant, and $\mathbf{q}$ is the heat flux. The ratio of parallel to perpendicular heat flux coefficients, $\kappa_\parallel/\kappa_\perp$, was set to 10^4–10^6, large

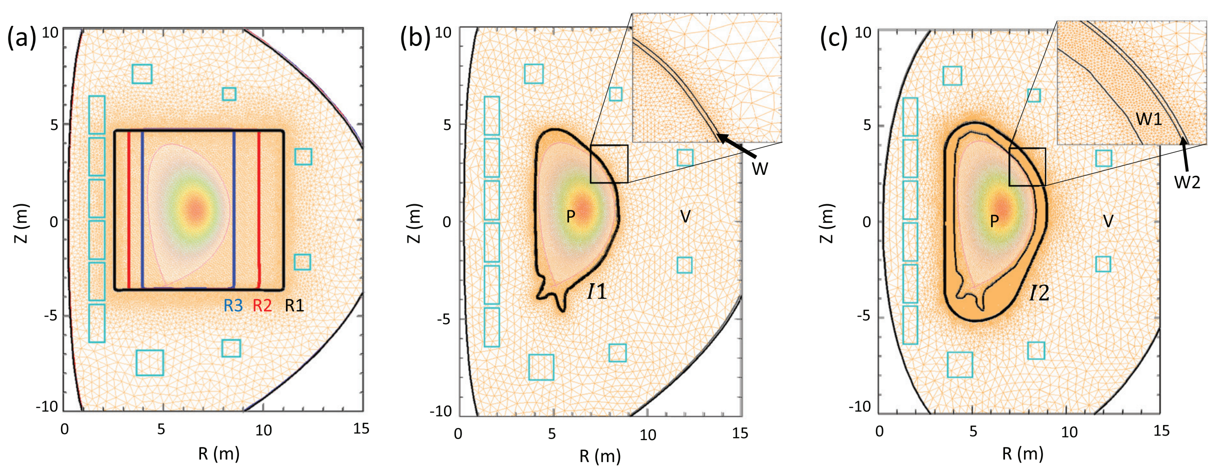

FIG. 1. Different wall geometries, computational domains, and meshes employed for the simulations. In all cases, the computational domain includes a plasma region (P), a wall region (W), and a vacuum region (V). (a) shows three different rectangular walls labeled as R1, R2, and R3, (b) shows a thin ITER first wall model $I1$, and (c) shows a two layer ITER vessel model, $I2$, in which the $W1$ region represents the first wall and blanket modules, and the $W2$ region, which is on average $\sim$60 cm away from the first wall contour, represents the inner shell of the ITER vacuum vessel.

enough to minimize the magnitude of halo currents, which were not considered in Ref. 5.

III. TOP–BOTTOM FLAT-PLATES WALL LIMIT

Here, we summarize some of the results presented in Ref. 5 that will be useful in this work. Following that model, which we will refer to as the flat-plates wall limit, the vertical displacement can be written as

$$\delta = 0 \qquad (I > I_*), \tag{2a}$$

$$\frac{\delta^2}{b^2} = 1.2158\left(\frac{I_*}{I} - 1\right) \qquad (I < I_*), \tag{2b}$$

where $\delta = Z_m(t) - Z_m(0)$ is the displacement of the magnetic axis measured from its initial equilibrium position and b is the top/bottom wall distance measured from the same equilibrium magnetic axis position. Equation (2b) has real solution when the plasma current has decayed below a critical current value I_*. When $I > I_*$ the solution is stable at $\delta = 0$. We can compute this critical current value by specifying the height b_{x0} of the x-point, at which the radial magnetic field vanishes, obtaining

$$\frac{I_0}{I_*} = 1.2337\frac{b_{x0}^2}{b^2}. \tag{3}$$

This result shows that $I_* < I_0$ only when the ratio $b_{x0}/b > 0.9$.

Therefore, in order to observe in our simulations a transition in which the plasma changes its equilibrium position from $\delta = 0$ to $|\delta| \neq 0$ when the plasma current decays below I_*, we have to choose the top/bottom walls close enough to the x-points. In addition, to make the comparison with the flat-plates wall limit, the top/bottom walls should be both equidistant to the equilibrium magnetic axis z-position $Z_m(0)$ and the side walls should be as far as possible from the plasma. That is why we used the R1 geometry shown in Fig. 1(a).

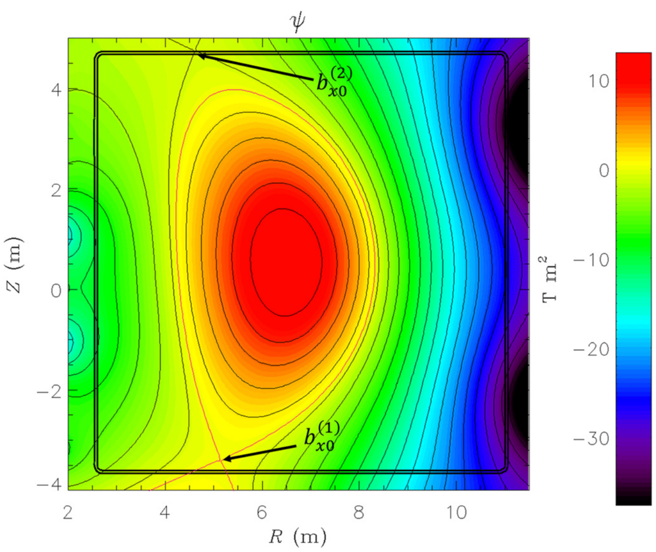

FIG. 2. ITER equilibrium poloidal flux employed is identical in all the cases, but different wall geometries were employed (as indicated in Fig. 1). Here, we show with the R1 model that was used to approximate the two flat perfect conducting plates.

Figure 2 shows the equilibrium poloidal flux ψ with contour lines. It also shows the two, active and passive, x-points. The theoretical model presented in Ref. 5 assumes up/down symmetry, but the ITER equilibrium is not. From Fig. 2, we get that $b_{x0}^{(1)}/b = 0.95$ and $b_{x0}^{(2)}/b \approx 1$, leading to $I_*^{(1)} = 13.5$ MA and $I_*^{(2)} = 12.2$ MA, respectively. From the analysis performed for the symmetric case, we infer from this that the configuration will certainly be unstable when the plasma current decays below 12.2 MA.

In order to compare with the flat-plates wall limit model, we evolved this initial equilibrium increasing the plasma Spitzer resistivity by 10^5 to simulate the current quench. Figure 3 shows the magnetic axis Z-position as a function of the plasma current, for slightly different but small perpendicular heat flux coefficients $\kappa_\perp$ ($\kappa_\parallel$ was fixed to 200). To get κ in SI units, multiply by $1.542 \times 10^{26}\ \mathrm{m}^{-1}\,\mathrm{s}^{-1}$. The artificial increase in the Spitzer resistivity produces a current quench (CQ) without a thermal quench (TQ). This keeps the plasma β approximately constant, avoiding the inward displacement and initial kick that triggers the VDE (as used, for example, in Ref. 7). The plasma β and $R-$ coordinate of the magnetic axis, R_m, are shown in Fig. 4 as a function of the plasma current. The perpendicular heat flux coefficient $\kappa_\perp$ was slightly varied in order to scan over small β variations, primarily due to the increased Ohmic heating when the resistivity is increased. We can observe from Fig. 3 that the simulation is in excellent agreement with the flat-plates wall limit model. It was not possible to generate a case that surpasses this stability limit using the R1 rectangular wall.

However, if the side walls are brought closer to the plasma, the stability of the $\delta = 0$ solution improves drastically. Figure 5 shows the case "(iv)" of Fig. 3 ($\kappa_\perp = 5 \times 10^{-5}$) for the R1 model but now compared with the R2 and R3 models. The side walls, which were neglected in Ref. 5, are seen to be very stabilizing to the VDE. They impose a constraint on the normal component of the perturbed magnetic field and, hence, on the plasma motion.

IV. COLD VDE DRIVEN BY A THERMAL QUENCH

In a more realistic situation, a cold VDE is triggered by a thermal quench (TQ). This produces a collapse in the plasma β and

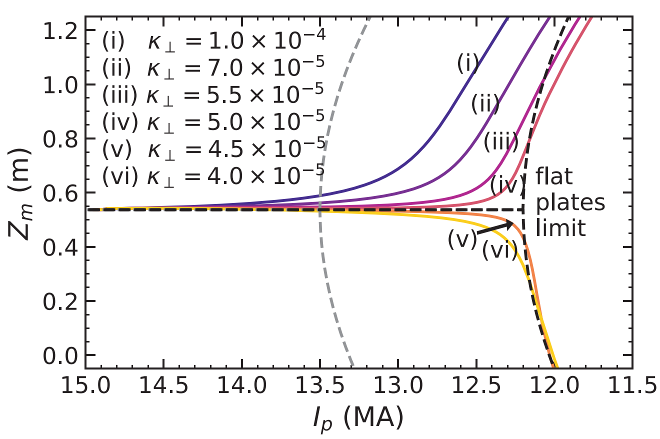

FIG. 3. $Z-$ coordinate of the magnetic axis as a function of the plasma current for different perpendicular heat flux coefficients $\kappa_\perp$. The dashed curves show the flat-plates wall limit model, Eq. (2).

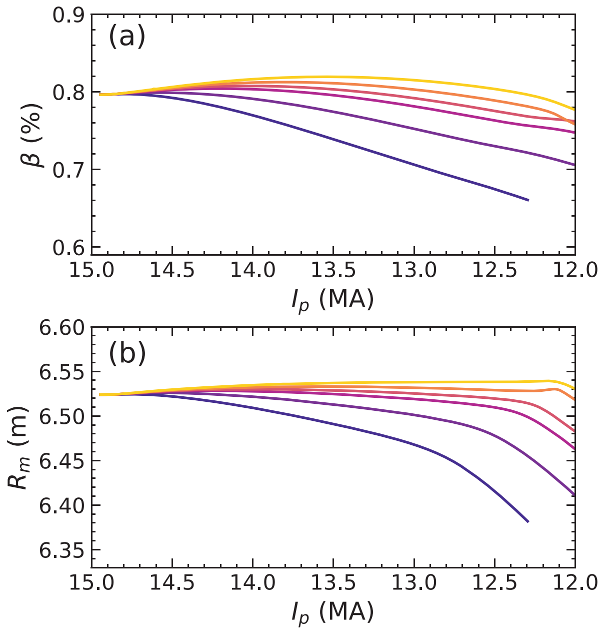

FIG. 4. (a) Plasma β and (b) $R-$ coordinate of the magnetic axis as a function of the plasma current for different perpendicular heat flux coefficients $\kappa_\perp$, as indicated in Fig. 3.

temperature, as shown in Fig. 6, which usually triggers the vertical displacement. Here, we have chosen a post-TQ $T_e \approx 30$ eV as a standard post-TQ plasma core temperature. The TQ is induced in the simulations by setting $\kappa_\perp$ to a large enough value. Different values lead to different post-TQ peak temperatures, as explained in Ref. 7. Here we used $\kappa_\perp = 4.8 \times 10^{-2}$. During this collapse, which in these simulations lasts $\lesssim$0.3 ms, the plasma changes its equilibrium state to satisfy the force-free condition and the evolution of this new state will be affected by the boundary condition imposed by the conducting walls. The evolution of some relevant global quantities is shown in Fig. 7. We can observe that in these cases, the R1 and R2 wall geometries lead to a significant upward motion, as shown in Fig. 7(a), while bringing the wall closer such as in R3 and *I*1 geometries substantially reduces the displacement.

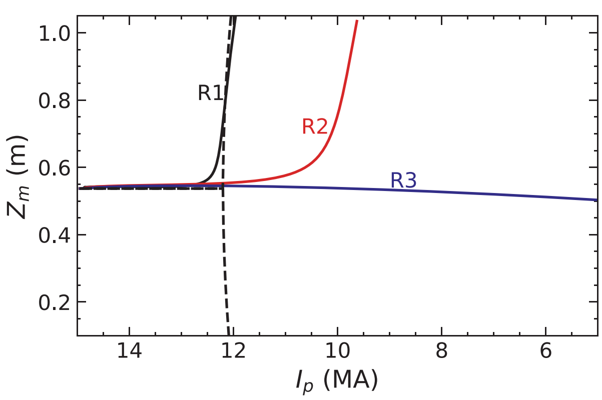

FIG. 5. $Z-$ coordinate of the magnetic axis as a function of the plasma current for different rectangular walls, as shown in Fig. 1(a).

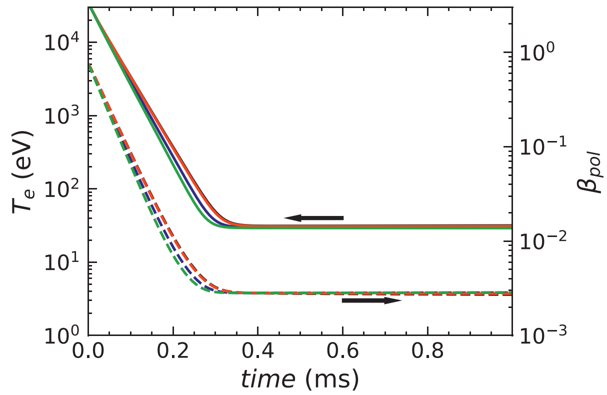

FIG. 6. Central electron temperature and plasma poloidal beta as a function of time for different wall geometries.

However, the nature of this upward/downward movement is different from that of a standard VDE, which exhibits exponential growth on the resistive wall timescale. Here, the vertical movement is a function of the plasma current and radial position. If the side walls are far enough away, such as in the R1 and R2 cases, the plasma will displace into a region where the external fields are more destabilizing. The combination of the stronger destabilizing force from the external fields and the weaker passive stabilization due to the reduced current will cause the configuration to seek a new equilibrium state, displaced vertically. It is seen that the R1 and R2 configurations displace vertically even before the plasma current begins to decrease. Freezing the plasma current (at a given major radius position) at any later time leads to a constant Z_m time evolution (an example is shown in Sec. V). In this sense, these simulations show an extension of the flat-plates wall limit for different wall geometries.

Figure 7(c) shows the current quench for all different cases. The current quench is affected not only by the plasma temperature after the TQ, which is almost identical in all cases ($\sim$30 eV), but also by the wall geometry. Different wall geometries allow the plasma to change its internal inductance in different ways, as shown in Fig. 7(d), in order to keep the magnetic fluxes constant and to satisfy their respective boundary condition.

V. THE ITER CASE

Figure 7 shows that the perfectly conducting ITER first wall limit (model *I*1) is the most stable case we scanned. A longer time history of the $Z-$ coordinate of the magnetic axis and plasma current is shown in Fig. 8. We can observe that the plasma is stable at $\delta = 0$ far beyond the flat-plates wall limit and goes to a solution $|\delta| \neq 0$ when the plasma current is below $\sim$2 MA. This result leads to an edge safety factor increasing in time as shown in Fig. 9, improving the stability of non-axisymmetric modes. On the other hand, we also include in Fig. 8 the results from the thicker wall model *I*2 shown in Fig. 1(c), in which the perfect conductor is assumed to be the outer wall layer *W*2, which accounts for the inner shell of the ITER vacuum vessel. Since this perfectly conducting wall is further away than in model *I*1, we can observe that the plasma is displaced from the very beginning, as the plasma current decreases. However, the vertical displacement is not as fast as in the flat-plates wall limit so that the edge safety factor, shown in Fig. 9, remains above 2 until the current has decayed below 6 MA. The dotted line in Fig. 8 exemplifies a case in which the current

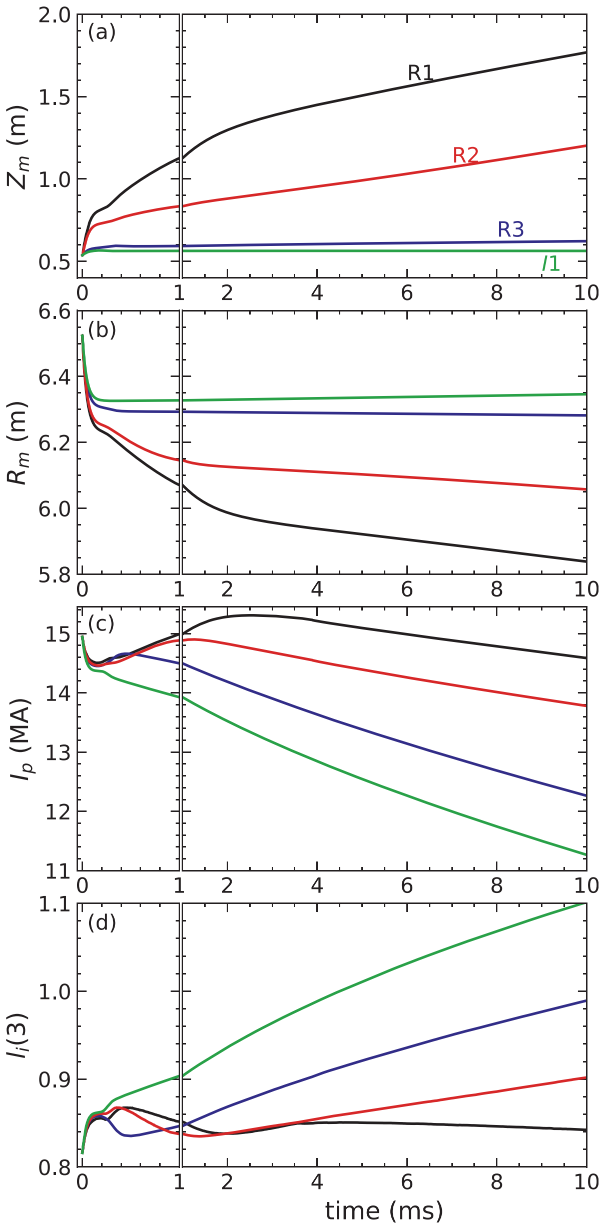

FIG. 7. Global quantities as a function of time for different wall models: (a) $Z-$ coordinate and (b) $R-$ coordinate of the magnetic axis, (c) plasma current, and (d) internal inductance. A zoom in time at the beginning shows the initial displacement caused by the thermal quench.

quench was frozen at an arbitrary time (~30 ms) by reducing the plasma resistivity. We can observe here that, as a consequence, Z_m also freezes in time, illustrating that the $Z-$ position is a function of the plasma current.

VI. CONCLUSIONS

In this work, we used the extended-MHD code M3D-C[1] and explored the perfectly conducting wall limit of an ITER cold VDE. We

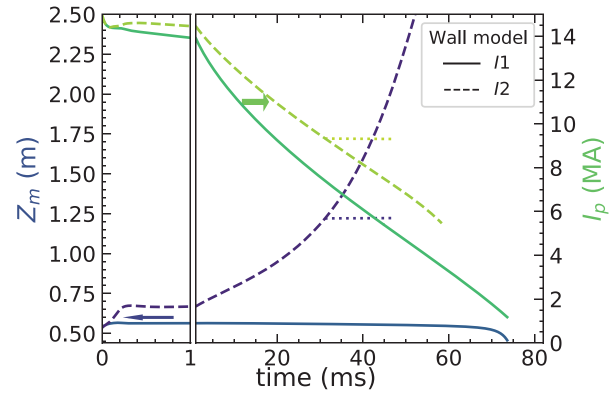

FIG. 8. Time evolution of the $Z-$ coordinate of the magnetic axis and plasma current for models *I*1 (solid) and *I*2 (dash). See Fig. 1 for models' reference. The dotted line shows that when freezing the current quench (by reducing the plasma resistivity), Z_m also freezes in time.

analyzed the flat-plates wall model by Boozer, performing a scan over different rectangular first wall geometries. We found that the model is applicable in a situation when the side walls are far enough from the plasma, but bringing the walls closer considerably improves the stability of the $\delta = 0$ solution. It is shown that in the case of the ITER first wall, the $\delta \neq 0$ solution takes place only when the plasma current has decayed below 2 MA.

Finally, when using the inner shell of the ITER vacuum vessel as a perfect conductor, the vertical displacement occurs at the time of the thermal quench, but it is a slow enough function of the current decay, compared to the flat-plates wall limit, so that the edge safety factor does not decrease significantly down to values below 2 until the current has decayed below 6 MA.

In all the simulated cases, it was found that, in the limit of a perfectly conducting wall, the vertical displacement showed a strong dependency on the plasma current, in agreement with a similar finding in the flat-plates wall limit. Freezing the current leads to a freezing of the magnetic axis position in contrast to "hot" VDEs, which begin with full plasma current and beta values and do not occur in the limit of a perfectly conducting wall. The findings in this paper appear to be

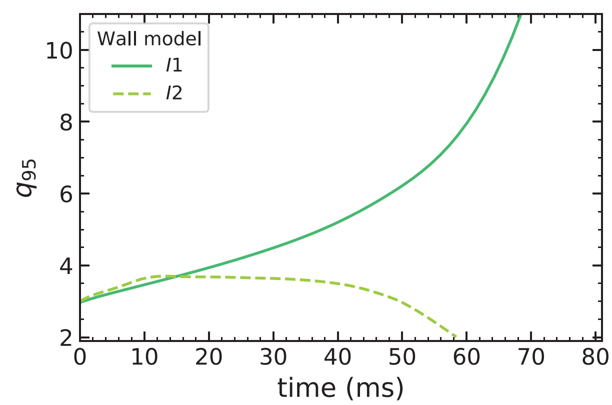

FIG. 9. Edge safety factor (q_{95}) as a function of time for wall models *I*1 (solid) and *I*2 (dash). See Fig. 1 for models' reference.

consistent with Ref. 2, although they did not consider realistic ITER plasma and vessel shapes, and did not take the ideal wall limit as was done here.

ACKNOWLEDGMENTS

This work was supported by the U.S. Department of Energy under DOE Contract No. DE-AC02–09CH11466 and the SciDAC CTTS. The authors are also grateful to Allen Boozer for fruitful discussions and to Fabio Villone for his help in defining the ITER vessel.

DATA AVAILABILITY

The data that support the findings of this study are available in the Princeton University DataSpace, Ref. 16.

REFERENCES

[1] A. H. Boozer, Phys. Plasmas **19**, 058101 (2012).
[2] D. I. Kiramov and B. N. Breizman, Phys. Plasmas **25**, 092501 (2018).
[3] A. Raffray, B. Calcagno, P. Chappuis, Z. Fu, A. Furmanek, C. Jiming, D.-H. Kim, S. Khomiakov, A. Labusov, A. Martin, M. Merola, R. Mitteau, S. Sadakov, M. Ulrickson, and F. Zacchia, Nucl. Fusion **54**, 033004 (2014).
[4] R. Roccella, S. Chiocchio, G. Janeschitz, M. Lehnen, V. Riccardo, M. Roccella, G. Sannazzaro, and JET Contributors, in 26th IAEA Fusion Energy Conference, Kyoto, Japan (2016), p. EX/P6–40.
[5] A. H. Boozer, Phys. Plasmas **26**, 114501 (2019).
[6] S. Jardin, F. Villone, C. Clauser, N. Ferraro, N. Isernia, G. Rubinacci, and S. Ventre, in *ECA: 46th EPS Conference on Plasma Physics* (EPS, Milan, 2019), Vol. 43C, p. P5.1003.
[7] C. Clauser, S. Jardin, and N. Ferraro, Nucl. Fusion **59**, 126037 (2019).
[8] J. Breslau, N. Ferraro, and S. Jardin, Phys. Plasmas **16**, 092503 (2009).
[9] S. C. Jardin, N. Ferraro, J. Breslau, and J. Chen, Comput. Sci. Discovery **5**, 014002 (2012).
[10] N. M. Ferraro, S. C. Jardin, L. L. Lao, M. S. Shephard, and F. Zhang, Phys. Plasmas **23**, 056114 (2016).
[11] D. Pfefferlé, N. Ferraro, S. C. Jardin, I. Krebs, and A. Bhattacharjee, Phys. Plasmas **25**, 056106 (2018).
[12] C. Sovinec, A. Glasser, T. Gianakon, D. Barnes, R. Nebel, S. Kruger, D. Schnack, S. Plimpton, A. Tarditi, and M. Chu, J. Comput. Phys. **195**, 355 (2004).
[13] M. Hölzl, P. Merkel, G. T. A. Huysmans, E. Nardon, E. Strumberger, R. McAdams, I. Chapman, S. Günter, and K. Lackner, J. Phys. **401**, 012010 (2012).
[14] I. Krebs, F. J. Artola, C. R. Sovinec, S. C. Jardin, K. J. Bunkers, M. Hoelzl, and N. M. Ferraro, Phys. Plasmas **27**, 022505 (2020).
[15] N. Ferraro, B. Lyons, C. Kim, Y. Liu, and S. Jardin, Nucl. Fusion **59**, 016001 (2019).
[16] Dataset: C. F. Clauser (2021). "ITER cold VDEs in the limit of perfectly conducting walls," Princeton University. http://arks.princeton.edu/ark:/88435/dsp015425kd34n